

RESEARCH

Open Access



# Stretch-activated current in human atrial myocytes and Na<sup>+</sup> current and mechano-gated channels' current in myofibroblasts alter myocyte mechanical behavior: a computational study

Heqing Zhan<sup>1\*</sup> , Jingtao Zhang<sup>2</sup>, Anquan Jiao<sup>1</sup> and Qin Wang<sup>1</sup>

\*Correspondence:

zhq86zijing@163.com

<sup>1</sup> College of Medical Information, Hainan Medical University, Haikou 571199, China

Full list of author information is available at the end of the article

## Abstract

**Background:** The activation of stretch-activated channels (SACs) in cardiac myocytes, which changes the phases of action potential repolarization, is proven to be highly efficient for the conversion of atrial fibrillation. The expression of Na<sup>+</sup> current in myofibroblasts (Mfbs) regenerates myocytes' action potentials, suggesting that Mfbs play an active role in triggering cardiac rhythm disturbances. Moreover, the excitation of mechano-gated channels (MGCs) in Mfbs depolarizes their membrane potential and contributes to the increased risk of post-infarct arrhythmia. Although these electrophysiological mechanisms have been largely known, the roles of these currents in cardiac mechanics are still debated. In this study, we aimed to investigate the mechanical influence of these currents via mathematical modeling. A novel mathematical model was developed by integrating models of human atrial myocyte (including the stretch-activated current, Ca<sup>2+</sup>-force relation, and mechanical behavior of a single segment) and Mfb (including our formulation of Na<sup>+</sup> current and mechano-gated channels' current). The effects of the changes in basic cycle length, number of coupled Mfbs and intercellular coupling conductance on myocyte mechanical properties were compared.

**Results:** Our results indicated that these three currents significantly regulated myocyte mechanical parameters. In isosarcometric contraction, these currents increased segment force by 13.8–36.6% and dropped element length by 12.1–31.5%. In isotonic contraction, there are 2.7–5.9% growth and 0.9–24% reduction. Effects of these currents on the extremum of myocyte mechanical parameters become more significant with the increase of basic cycle length, number of coupled Mfbs and intercellular coupling conductance.

**Conclusions:** The results demonstrated that stretch-activated current in myocytes and Na<sup>+</sup> current and mechano-gated channels' current in Mfbs significantly influenced myocyte mechanical behavior and should be considered in future cardiac mechanical mathematical modeling.



**Keywords:** Mechano-gated channels (MGCs), Myocyte mechanics, Mathematical modeling, Myofibroblast–myocyte (Mfb–M) coupling, Stretch-activated channels (SACs), Voltage-gated sodium channels (VGSCs)

## Background

As an alternative of experimental studies, computational modeling studies provide a powerful framework for gaining substantial insights of cardiac electrophysiology and mechanics in many aspects [1, 2]. For cardiac electrophysiological simulation, cardiac cell action potential (AP) models are built to represent current flow through ion pumps, channels, and exchangers [3, 4]. For mechanical simulation, the active stress/strain models and Hill's three-element model have been formulated to lay out active contraction [5, 6].

Cardiac electrical activities have intimate connection with mechanical actions. The interaction between them is referred as electromechanical coupling (EMC) and mechano-electrical feedback (MEF) [7]. As a major mechanism of the MEF, the stretch-activated channel (SAC) has been used to explain changes in electrophysiological behavior by mechanical deformation. Several cellular experimental and modeling studies have examined the impact of SACs on cardiac electrophysiology [8–11].

Recently, clinical data and simulation studies have provided some important insights into cardiac structural remodeling, especially fibrosis as a hallmark of permanent atrial fibrillation. Many of them verified that both fibroblasts and myofibroblasts (Mfbs) modulated cardiac electrical conduction, coordinated tissue remodeling, and integrated signals [12–14]. They have been considered as active communicators rather than non-excitable cells, which involve several currents like cardiac myocytes, e.g., the currents through potassium channels [15, 16], the non-selective transient receptor potential cationic channel subfamily M member 7 (TRPM7) [17], voltage-gated sodium channels (VGSCs) [18, 19], chloride channels [20], single mechano-gated channels (MGCs) [21], and voltage-dependent proton currents [22].

Computational models of atrial fibrosis have been used to investigate how fibroblasts modulate cardiac myocyte electrophysiology. At the cellular level, processes of fibrotic remodeling are represented as fibroblast proliferation and phenotype switching [23, 24]. Simulation results showed that coupling of fibroblasts or Mfbs to atrial myocytes resulted in shorter duration of the action potential (APD), slower conduction, and spiral wave breakups [25–28].

As a critical determinant of cardiac mechanics, fibroblast-mediated changes in extracellular matrix structure are also investigated by computational modeling. Cell compaction of collagen gels has been studied by explicitly calculating the mechanical equilibrium between each cell's contractile forces and nearby collagen fibers' mechanical properties [29, 30]. Infarct mechanics has been simulated by coupling agent-based model predictions to a finite element model [31, 32]. These studies have found that fibroblast alignment parallel to a strain cue provides a negative feedback to radical changes in local fiber orientations.

Previous studies mentioned above have examined cardiac myocyte functions in many aspects; however, no study to the our best knowledge has considered the following two aspects in Mfb–myocyte (Mfb–M) coupling, especially in EMC: (1) the

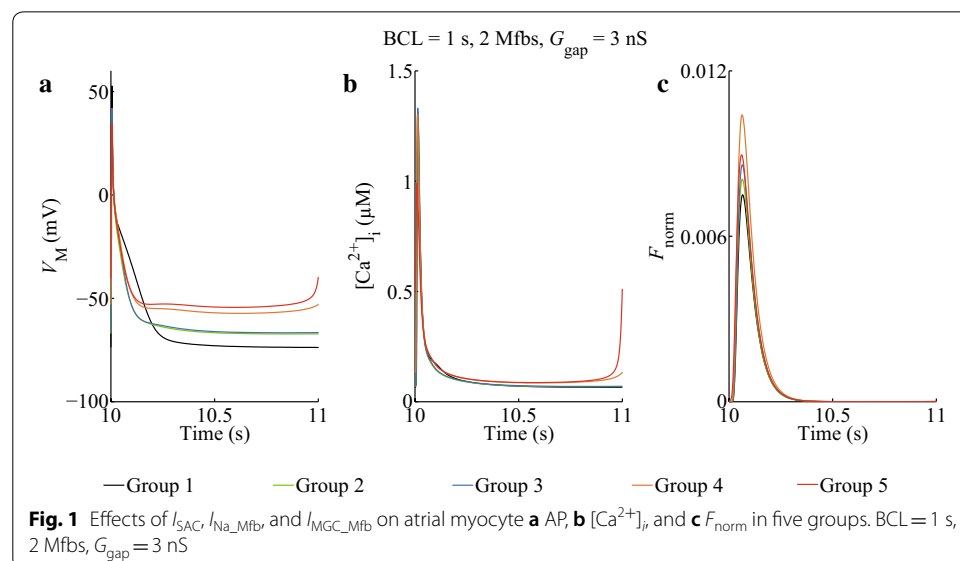
stretch-activated ion channel current ( $I_{SAC}$ ) in myocytes, which influences cardiac myocytes electrophysiological characteristics under stretching [33, 34]; (2) the currents through VGSCs ( $I_{Na\_Mfb}$ ) and MGCs ( $I_{MGC\_Mfb}$ ) in Mfbs, which could influence Mfb properties and contribute to EMC in cardiac pathologies [18, 21].

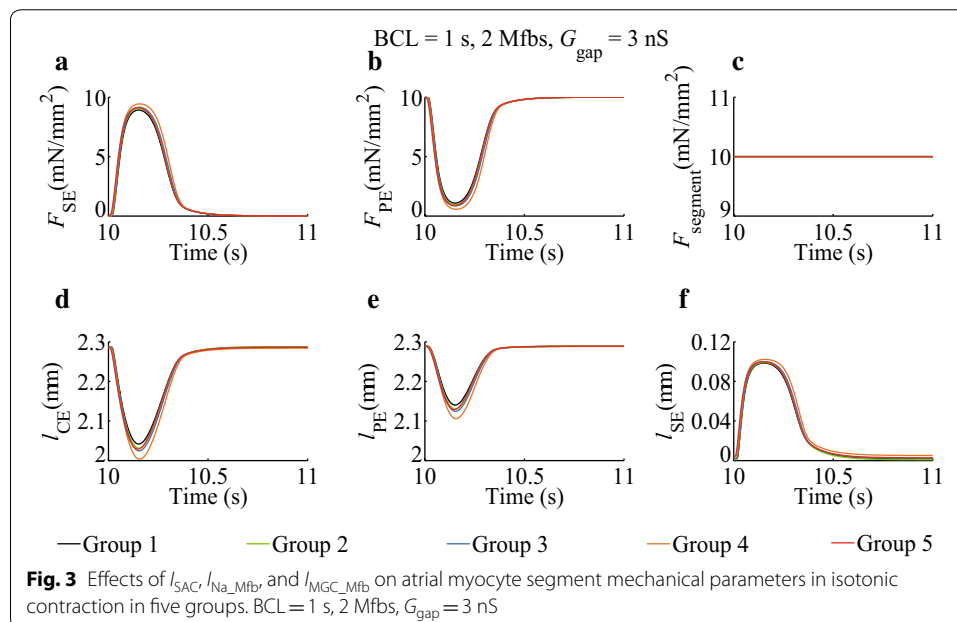
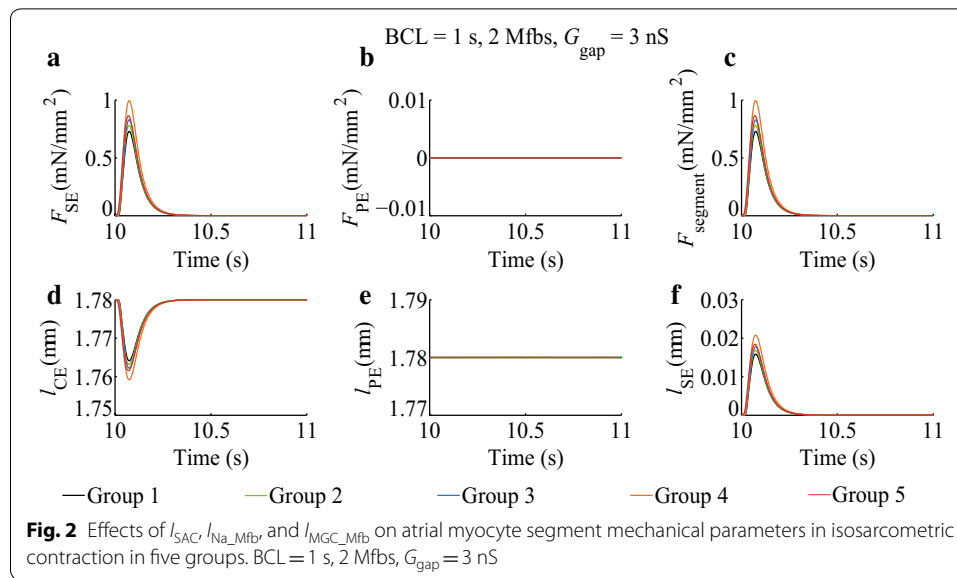
Our previous study has found that  $I_{Na\_myofb}$  and  $I_{MGC\_Mfb}$  regenerated APs in myocytes and Mfbs [28]. In this study, we aimed to investigate the role of  $I_{SAC}$ ,  $I_{Na\_Mfb}$ , and  $I_{MGC\_Mfb}$  in the mechanical contraction of cardiac myocyte. Simulation results of human atrial myocyte segment mechanical dynamics with different gap-junctional conductance ( $G_{gap}$ ), number of coupled Mfbs and basic cycle lengths (BCLs) were examined.

## Results

### Effects of $I_{SAC}$ , $I_{Na\_Mfb}$ , and $I_{MGC\_Mfb}$ on atrial myocyte AP, $[Ca^{2+}]_i$ , and the normalized force

Figure 1 shows the combinational effects in five groups (see “Simulation protocol” section) of  $I_{SAC}$ ,  $I_{Na\_Mfb}$ , and  $I_{MGC\_Mfb}$  on the membrane potential, intracellular  $Ca^{2+}$  concentration and the normalized force ( $F_{norm}$ ) of myocytes with a  $G_{gap}$  of 3 nS and a BCL of 1 s. For myocytes, coupling Mfbs (Group 2-5) resulted in gradual decrease of myocyte membrane potential amplitude ( $V_{max}$ ) and APD at 90% repolarization (APD<sub>90</sub>), and increase of the resting myocyte membrane potential ( $V_{rest}$ ) depolarization (Fig. 1a). Meanwhile, a spontaneous excitement was emerged in Group 5, in which the peak  $[Ca^{2+}]_i$  dropped significantly (Fig. 1b), indicating that  $I_{SAC}$ ,  $I_{Na\_Mfb}$ , and  $I_{MGC\_Mfb}$  could result in discordant alternans. From the traces of  $F_{norm}$  (Fig. 1c), it can be observed that the peak  $F_{norm}$  increased after myocyte coupled to Mfbs. It was increased by 7.6% (Group 2), 14.5% (Group 3), 38.7% (Group 4), and 19.2% (Group 5) as compared to the control (Group 1). It was remarkable that Group 4 got the biggest  $F_{norm}$  increment, which meant  $F_{norm}$  of myocytes could be significantly enhanced by the combination of  $I_{SAC}$  and  $I_{Na\_Mfb}$ . However, the increment relatively declined in





Group 5 with the introduction of  $I_{MGC\_Mfb}$ . This might suggest that deformation in myocytes enhanced  $F_{norm}$ , while in Mfbs the deformation relatively hindered it. The effects of  $I_{SAC}$  and  $I_{MGC\_Mfb}$  on the force of atrial myocytes were opposite, with  $I_{SAC}$  increasing and the other one decreasing.

#### Effects of $I_{SAC}$ , $I_{Na\_Mfb}$ , and $I_{MGC\_Mfb}$ on atrial myocyte segment mechanical parameters

Traces of  $F_{SE}$ ,  $F_{PE}$ ,  $F_{segment}$ ,  $l_{CE}$ ,  $l_{PE}$ , and  $l_{SE}$  obtained in five groups for the simulations of isosarcometric contraction with sarcomere length of 1.78  $\mu$ m are displayed in Fig. 2, and the ones for simulations of isotonic contraction with applied force of 10 mN per square millimeter ( $mN/mm^2$ ) are displayed in Fig. 3.

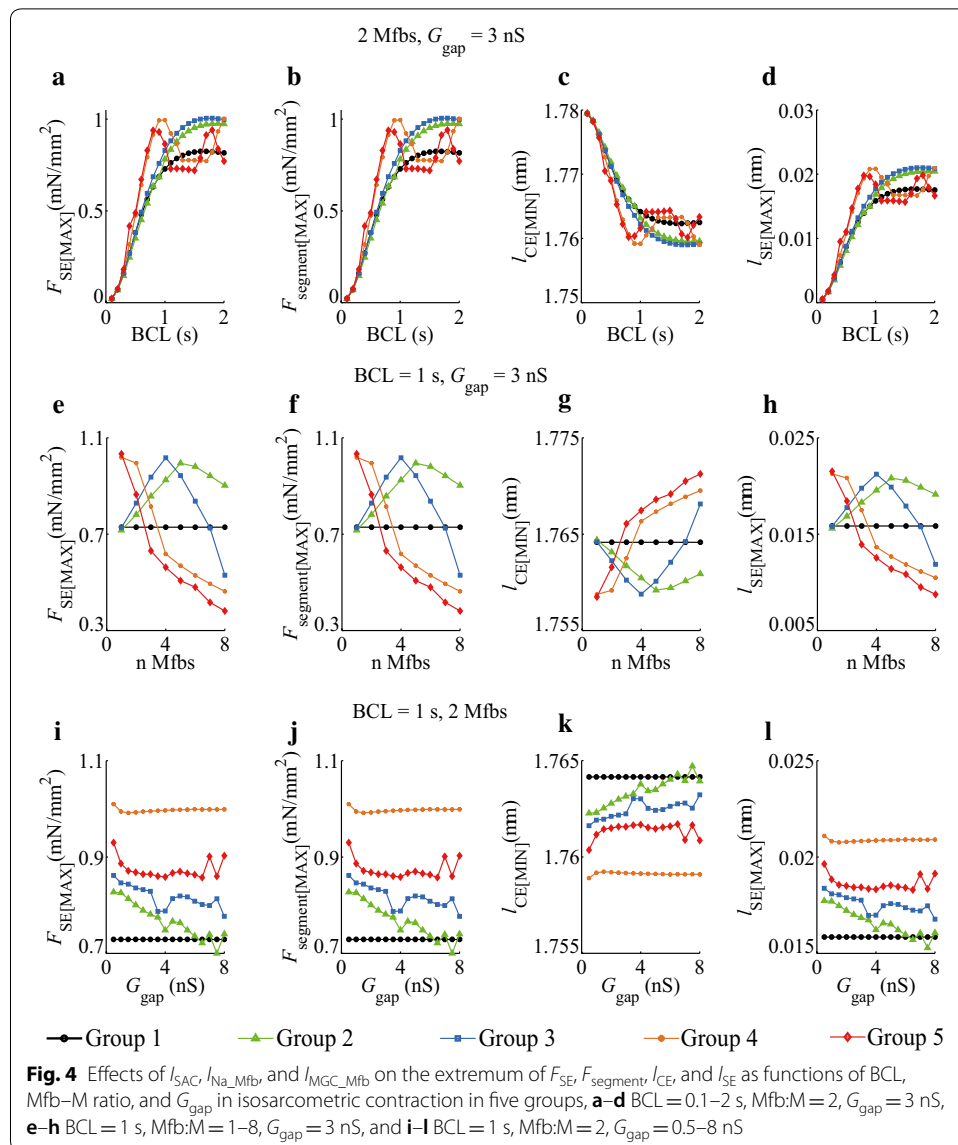
In isosarcometric contraction (Fig. 2),  $F_{PE}$  and  $l_{PE}$  in five groups were constant. Peak  $F_{SE}$  increased when myocyte coupled to Mfbs. It was increased by 7.2% (Group 2), 13.8% (Group 3), 36.6% (Group 4), and 18.5% (Group 5) as compared to the control (Group 1). Using Eq. (14) (see “Mechanical behavior of a single segment” section), the increments in  $F_{segment}$  were the same as those in  $F_{SE}$ . On the contrary,  $l_{CE}$  decreased when myocyte coupled to Mfbs. The minimum of  $l_{CE}$  was dropped by 6.4% (Group 2), 12.1% (Group 3), 31.5% (Group 4), and 16.2% (Group 5) as compared to the control (Group 1). Using Eq. (15), the changes in  $l_{CE}$  were equal to those in  $l_{SE}$ . Similar to Fig. 1, Group 4 had the most significant change, indicating that the combination of  $I_{SAC}$  and  $I_{Na\_Mfb}$  played a significant role in determining myocyte segment mechanical behavior.

In isotonic contraction (Fig. 3),  $F_{segment}$  in five groups was constant. Like Fig. 2a, the peak value of  $F_{SE}$  also increased when Mfbs were coupled. It was increased by 1.6% (Group 2), 2.7% (Group 3), 5.9% (Group 4), and 2.5% (Group 5) as compared to the control (Group 1). The increments were smaller than those in isosarcometric contraction. According to Eq. (14), the decrements in  $F_{PE}$  were equal to the increments in  $F_{SE}$ . The minimum of  $l_{CE}$  was dropped by 4.3% (Group 2), 7.4% (Group 3), 15.8% (Group 4), and 6.3% (Group 5) as compared to the control (Group 1), while the peak value of  $l_{SE}$  was increased by 0.6%, 1.4%, 3.7%, and 0.9%, and finally,  $l_{PE}$  were declined by 6.8%, 11.4%, 24.0%, and 10.0%.  $I_{SAC}$ ,  $I_{Na\_Mfb}$ , and  $I_{MGC\_Mfb}$  not only changed the extreme values of  $l_{CE}$ ,  $l_{PE}$ , and  $l_{SE}$ , but also altered  $l_{CE}$  and  $l_{SE}$  in the resting stage. For example, the value of  $l_{SE}$  in resting period was 0.0021  $\mu\text{m}$  (Group 1), 0.0013  $\mu\text{m}$  (Group 2), 0.0021  $\mu\text{m}$  (Group 3), 0.0051  $\mu\text{m}$  (Group 4), and 0.0032  $\mu\text{m}$  (Group 5), respectively. Similarly, Group 4 has the most impact on the mechanical parameters.

To investigate the effects of  $I_{SAC}$ ,  $I_{Na\_Mfb}$ , and  $I_{MGC\_Mfb}$  on the extreme values of atrial myocyte segment mechanical parameters, we simulated five groups with different BCLs, Mfb–M ratios, and  $G_{gap}$  in both isosarcometric contraction (Fig. 4) and isotonic contraction (Fig. 5).

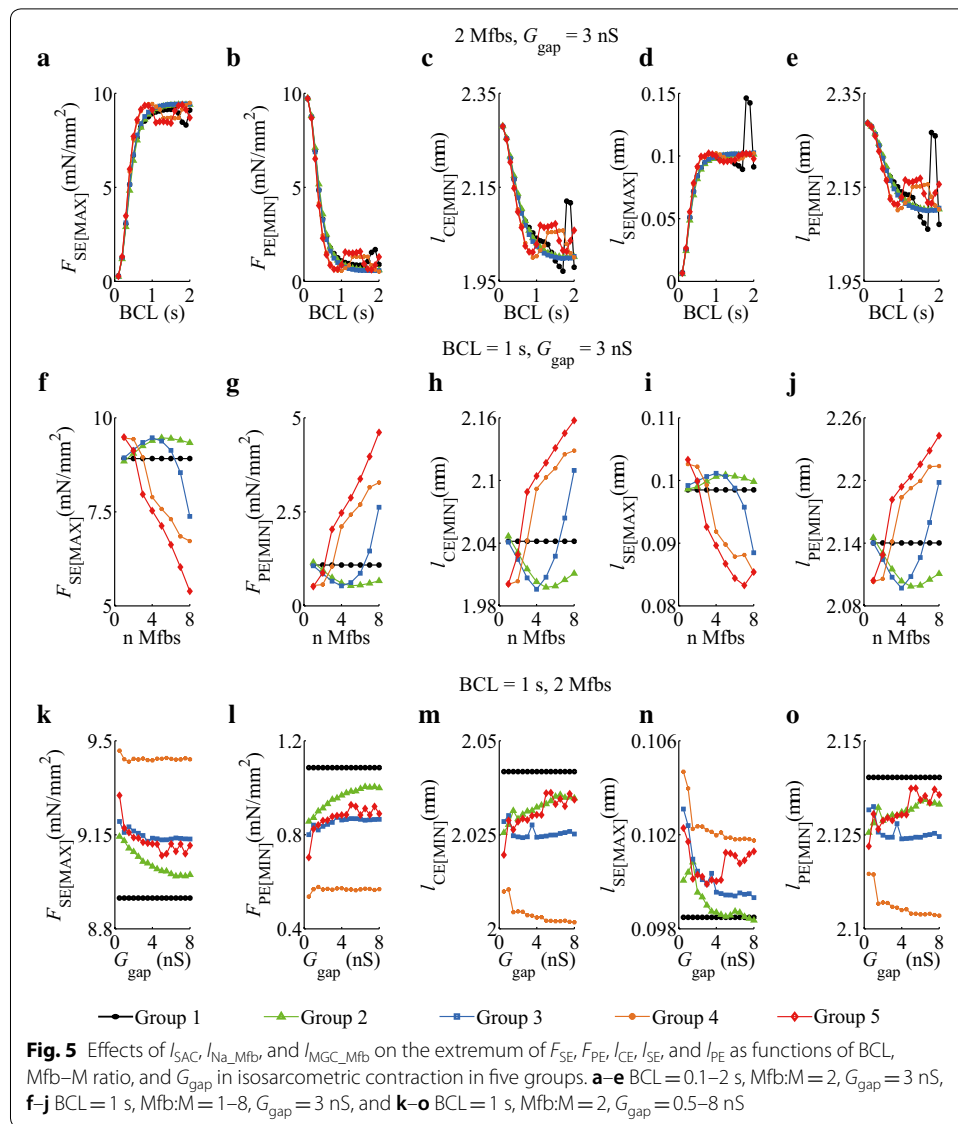
From the traces of the extremum of  $F_{SE}$ ,  $F_{segment}$ ,  $l_{CE}$ , and  $l_{SE}$  for BCL = 0.1–2 s (Fig. 4a–d), it could be observed that peak  $F_{SE}$  ( $F_{SE[ MAX ]}$ ), peak  $F_{segment}$  ( $F_{segment[ MAX ]}$ ), and peak  $l_{SE}$  ( $l_{SE[ MAX ]}$ ) increased, and valley value of  $l_{CE}$  ( $l_{CE[ MIN ]}$ ) decreased with increasing BCL, in isosarcometric contraction. When BCL was less than 1 s,  $F_{SE[ MAX ]}$ ,  $F_{segment[ MAX ]}$  and  $l_{SE[ MAX ]}$  at each BCL increased and  $l_{CE[ MIN ]}$  decreased in Groups 2–5 as compared to Group 1. Meanwhile, at each BCL,  $F_{SE[ MAX ]}$ ,  $F_{segment[ MAX ]}$ , and  $l_{SE[ MAX ]}$  in Group 4 reached their maximums, and  $l_{SE[ MAX ]}$  obtained its minimum. This suggests that  $I_{SAC}$  together with  $I_{Na\_Mfb}$  had the key influence on myocyte mechanical parameters. The influence disappeared in Group 5, suggesting that the role of  $I_{MGC\_Mfb}$  in myocytes was opposite compared to  $I_{SAC}$ . As BCL longer than 1 s, each parameter in Group 1 to 3 has increased or decreased as a same trend, whereas fluctuated in Group 4 and 5. These phenomena might be attributed to that  $I_{SAC}$  and  $I_{Na\_Mfb}$  enhanced atrial myocytes excitability and triggered spontaneous excitements at large BCLs.  $[Ca^{2+}]_i$ , the vehicle of EMC, also fluctuated, driving the undulation of mechanical behavior.

Figure 4e–h shows the extremum of four parameters with Mfb–M ratios ranging from 1 to 8. Parameters in Group 1 were constants as no Mfb was coupled to myocytes. Unlike the similar trends of five groups in Fig. 4a–d, the trends of Group 2 and Group 3 in Fig. 4e–h were close and mostly distributed over one side of Group 1, and



the trends of Group 4 and Group 5 were similar and distributed over the other side. Our results demonstrated that introducing currents through SACs in myocytes and currents through MGCs in Mfbs in cardiac modeling could lead to different simulation results. In fact, the stretch ability and contractility of myocytes in fibrotic heart were quite different from those in normal heart. Integrated  $I_{SAC}$  and  $I_{MGC\_Mfb}$  in cardiac simulation could help obtain more accurate and closer to experimental results.

Figure 4i–l shows the extremum of four parameters with  $G_{gap}$  ranging from 0.5 to 8 nS. Parameters in Group 1 were also constants. The variance of five groups was less than those in other settings (Fig. 4a–h), suggesting the relative small effects of  $G_{gap}$  on myocyte mechanical parameters. The traces of Group 2 to 5 were mostly distributed over one side of Group 1. Parameters at each  $G_{gap}$  in Group 4 got the highest or lowest value among five groups, and parameters in Group 5 took the second place, indicating that  $I_{SAC}$ ,  $I_{Na\_Mfb}$ , and  $I_{MGC\_Mfb}$  played a strong role in atrial myocyte mechanical behavior.



The extremum of  $F_{SE}$ ,  $F_{PE}$ ,  $l_{CE}$ ,  $l_{SE}$  and  $l_{PE}$  as functions of BCL, Mfb–M ratio, and  $G_{gap}$  in isotonic contraction are showed in Fig. 5.

In Fig. 5a–e, the parameters among five groups were close to each other. As BCL increased, the values in Group 1, 4 and 5 first increased and then decreased. In these groups, pure myocyte or integrating  $I_{SAC}$  and  $I_{MGC\_Mfb}$  in fibrotic myocyte were more likely to cause discordant alternans and mechanical parameters fluctuation at big BCLs.

In Fig. 5f–j, the parameters in Group 2 always stayed over one side of Group 1 as the coupled ratio increased, while the parameters in other groups finally converged over the other side. It suggested that integrating  $I_{SAC}$ ,  $I_{Na\_Mfb}$ , and  $I_{MGC\_Mfb}$  in fibrotic myocyte significantly influenced the myocyte segment mechanical behavior at large coupled ratios.

In Fig. 5k–o, the parameters in Group 1 were constant, and Group 2, 3, and 5 had the similar traces, while Group 4 got the highest or lowest values. Therefore,  $I_{SAC}$ ,  $I_{Na\_Mfb}$ , and  $I_{MGC\_Mfb}$  had relative influences on mechanical parameters at large  $G_{gap}$ .

## Discussion

This study investigated the roles of  $I_{SAC}$ ,  $I_{Na\_Mfb}$ , and  $I_{MGC\_Mfb}$  in myocyte segment mechanical behavior. To address these issues, computational simulations of the coupled Mfb–M system were performed by employing a combination of models of the human atrial myocyte (including  $I_{SAC}$ ) and Mfb (including  $I_{Na\_Mfb}$  and  $I_{MGC\_Mfb}$ ), as well as models of  $Ca^{2+}$ –force relation and myocyte mechanical segment. Specifically, effects of these currents with changes in (1) BCL, (2) the number of coupled Mfbs, and (3)  $G_{gap}$  on atrial myocyte segment mechanical parameters were investigated. The integration of  $I_{SAC}$ ,  $I_{Na\_Mfb}$ , and  $I_{MGC\_Mfb}$  could result in (1) decreased  $V_{max}$  and  $APD_{90}$ , increased  $V_{rest}$  depolarization, and spontaneous excitations even discordant alternans at large BCLs, and (2) increased peak value of  $F_{SE}$ ,  $F_{segment}$ , and  $l_{SE}$  and decreased valley value of  $l_{CE}$  in isosarcometric contraction, and increased peak value of  $F_{SE}$  and  $l_{SE}$  and decreased valley value of  $F_{PE}$ ,  $l_{CE}$ , and  $l_{PE}$  in isotonic contraction. Moreover,  $I_{SAC}$  and  $I_{MGC\_Mfb}$  have relative effects on myocyte segment mechanical parameters.

### Effects of $I_{SAC}$ , $I_{Na\_Mfb}$ , and $I_{MGC\_Mfb}$ on atrial myocyte segment mechanical properties

Effects of  $I_{SAC}$ ,  $I_{Na\_Mfb}$ , and  $I_{MGC\_Mfb}$  on the excitability of human atrial myocytes have been discussed in our previous study [28]. Here, we discussed the roles of these currents in myocyte segment mechanical behavior.

EMC and MEF were two known effects [7], but the physical role of MEF in EMC was still poorly understood. In general,  $I_{SAC}$  handling as the major mechanisms of the MEF, was reported to enhance the early phase of AP repolarization and prolong or delay the final phase of repolarization [9, 35, 36]. But the impact of  $I_{SAC}$  on cardiac mechanics, to our best knowledge, has been rarely studied so far. In our present study, the stretch-activated currents had the most significant influence on myocyte segment mechanical parameters in both isosarcometric contraction and isotonic contraction.

For cardiac Mfbs, many studies have verified that mechanical cues activated cardiac Mfbs and led to increased production of extracellular matrix [37, 38]. Mfbs were regarded as a critical determinant of cardiac mechanics. Previous studies have used computational modeling to demonstrate the acute mechanical effects on cardiac fibroblast structure and organization [39, 40]. They found that an axial strain environment could guide fibroblast proliferation, orientation, and migration [31, 41, 42]. Several groups have simulated cell compaction of collagen gels by calculating mechanical equilibrium between each cell's contractile forces and nearby collagen fibers' mechanical properties. They reported that cellular organization is tightly linked to the mechanical feedback loop between cells and matrix [29, 30]. These studies were all about the stretch-induced responses of quiescent cardiac Mfbs. However, the inverse process, i.e., the Mfbs-induced responses of cardiac mechanics, has not been widely explored. Our results showed that coupling Mfbs changed myocytes mechanical properties. In addition, we compared the results of before and after adding  $I_{Na\_Mfb}$  and  $I_{MGC\_Mfb}$  in the Mfb

model, and found that the effects of  $I_{MGC\_Mfb}$  on the force of atrial myocytes were contrary to  $I_{SAC}$ .

For  $I_{Na\_Mfb}$ , many studies have been conducted to investigate how this current could influence Mfb proliferation [18, 43]. Our results showed that  $I_{Na\_Mfb}$  decreased  $V_{max}$  and  $APD_{90}$  and increased  $V_{rest}$  depolarization in myocytes. This depolarization changed diastolic  $Ca^{2+}$  levels and then altered myocytes mechanical behavior.

For  $I_{MGC\_Mfb}$ , experimental data have indicated that cardiac fibroblasts expressed functional MGCs, contributing to the cardiac MEF both under physiological and pathophysiological conditions [44, 45]. We assumed that it could affect myocytes mechanical characteristics like  $I_{SAC}$ . Our results supported this hypothesis. In our simulations,  $I_{MGC\_Mfb}$  altered myocytes mechanical behavior. Interestingly, the effects of  $I_{MGC\_Mfb}$  and  $I_{SAC}$  on myocyte segment mechanical parameters seemed to be opposite. Myocytes stretch activated  $I_{SAC}$  and enhanced the influence on mechanical parameters, while Mfbs compression activated  $I_{MGC\_Mfb}$  and weakened the influence. Moreover, MGCs were activated by fibroblast compression and inactivated by fibroblast stretch [21], implying that  $I_{MGC\_Mfb}$  should be integrated in cell modeling only during cell compression, such as fibroblasts/Mfbs compression caused by stretching and dilatation of surrounding cardiac myocytes.

Mfb was a critical determinant of cardiac mechanics. Previous studies have demonstrated that abnormal quantity or organization of Mfb could lead to both systolic and diastolic dysfunction [12, 30, 46]. Besides, previous modeling work suggested that Mfb–M coupling contributed to arrhythmia formation [25, 47]. The key factors included BCL, the number of coupled Mfbs, and  $G_{gap}$ . Here, we integrated  $I_{Na\_Mfb}$ ,  $I_{SAC}$ , and  $I_{MGC\_Mfb}$  into Mfb–M coupling and compared their effects on myocyte mechanical properties in different settings of BCL, Mfb–M ratio, and  $G_{gap}$ . To the best of our knowledge, this has not been examined before. With BCL, Mfb–M ratio, and  $G_{gap}$  increasing, impacts of these currents on the extremum of myocyte mechanical parameters became greater, as summarized in Figs. 4 and 5.

## Limitations

Two limitations in the present study should be mentioned. First, functional roles of SACs in Mfbs were not considered. Direct proof of mechanoactivation of mechano-sensitive channels in cardiac Mfbs was limited. A handful of experimental studies have found that mechanical cues could lead to the opening of so-called SACs, and transient receptor potential canonical channels were candidates for the stretch-activated currents measured in cardiac fibroblasts [48, 49]. However, the current–voltage relation of  $I_{SAC}$  in Mfbs needs further study. Second, the breadth of this computational study needs to be extended. Our work focused on the scale of local cell–cell interactions. Other scales, such as scales of subcellular signaling, cell–matrix interactions, tissue remodeling, and organ level conduction properties, were not included in this preliminary study. In fact, processes across these scales did not occur in isolation but operated as an interconnected system with every level passing information to other levels. Therefore, multi-scale modeling frameworks still need to be developed, although they brought computational challenges, and such models involving cardiac Mfbs and fibrosis were still rare.

## Conclusions

This study demonstrated the combinational effects of  $I_{SAC}$  in myocytes and  $I_{Na\_Mfb}$  and  $I_{MGC\_Mfb}$  in Mfbs on myocyte mechanical properties. Our results showed that the addition of  $I_{SAC}$ ,  $I_{Na\_Mfb}$ , and  $I_{MGC\_Mfb}$  regulated the peak and valley values of myocyte mechanical parameters in both isosarcometric contraction and isotonic contraction. Effects of these currents on the extremum of myocyte mechanical parameters become more evident as BCL, Mfb–M ratio, and  $G_{gap}$  increased. The effects proved that the stretch-activated current in atrial myocyte and  $Na^+$  current and mechano-gated channels in Mfbs should be considered in future pathological cardiac mechanical mathematical modeling, such as atrial fibrillation and cardiac fibrosis.

## Methods

Mathematical model was developed by integrating (1) the model of the human atrial myocyte [50], (2) the model of  $I_{SAC}$  [33], (3) the model of  $Ca^{2+}$ –force relation [51, 52], (4) the active model of the human cardiac Mfb [26], (5) our proposed formulation of  $I_{Na\_Mfb}$  and  $I_{MGC\_Mfb}$  based on experimental findings from Chatelier et al. [18] and Kamkin et al. [21], and (6) the Hill three-element rheological scheme of a single segment of myocyte [53, 54]. In following sections, the details of each component of the model will be described.

### The model of Mfb–M coupling

The Mfb–M coupling will be modeled based on [26], with the differential equations for the membrane potential of cardiac Mfb and myocyte are given by

$$\frac{dV_{Mfb,i}}{dt} = -\frac{1}{C_{m,Mfb}} (I_{Mfb,i}(V_{Mfb,i}, t) + G_{gap}(V_{Mfb,i} - V_M)) \quad (1)$$

$$\frac{dV_M}{dt} = -\frac{1}{C_{m,M}} \left( I_M(V_M, t) + \sum_{i=1}^n G_{gap}(V_M - V_{Mfb,i}) \right), \quad (2)$$

where  $V_{Mfb,i}$  and  $V_M$  represent the transmembrane potential of the  $i$ th coupled Mfb and the human atrial myocyte,  $C_{m,Mfb}$  and  $C_{m,M}$  represent the membrane capacitance of the Mfb and the myocyte,  $I_{Mfb,i}$  and  $I_M$  represent the transmembrane current of the  $i$ th coupled Mfb and the human atrial myocyte, and  $G_{gap}$  represents the gap-junctional conductance. It is also noted that a negative  $I_{gap}$  [i.e.,  $G_{gap}(V_{Mfb,i} - V_M)$ ] indicates that the current is flowing from the myocyte into the  $i$ th Mfb, and  $n$  is the total number of coupled Mfbs.

### Mathematical model of the human atrial myocyte

The mathematical model of the human atrial myocyte developed by Maleckar et al. [50], which is based on experimental data and has correctly replicated APD restitution of the adult human atrial myocyte, was adopted in this study. To examine the influence of the stretch on myocyte AP, the original model from Maleckar et al. is modified with the total ionic current of myocyte ( $I_M$ ) given as

$$I_M(V_M, t) = I_{Na} + I_{CaL} + I_t + I_{Kur} + I_{K1} + I_{K,r} + I_{K,s} + I_{B,Na} + I_{B,Ca} + I_{NaK} + I_{CaP} + I_{NaCa} + I_{SAC} - I_{stim}, \quad (3)$$

where  $I_{Na}$  is fast inward  $Na^+$  current,  $I_{CaL}$  L-type  $Ca^{2+}$  current,  $I_t$  transient outward  $K^+$  current,  $I_{Kur}$  sustained outward  $K^+$  current,  $I_{K1}$  inward-rectifying  $K^+$  current,  $I_{K,r}$  rapid delayed rectifier  $K^+$  current,  $I_{K,s}$  slow delayed rectifier  $K^+$  current,  $I_{B,Na}$  background  $Na^+$  current,  $I_{B,Ca}$  background  $Ca^{2+}$  current,  $I_{NaK}$   $Na^+-K^+$  pump current,  $I_{CaP}$  sarcolemmal  $Ca^{2+}$  pump current,  $I_{NaCa}$   $Na^+-Ca^{2+}$  exchange current,  $I_{SAC}$  stretch-activated current, and  $I_{Stim}$  stimulated current.

### The model of $I_{SAC}$

Kuijpers et al. [55] have conducted experimental studies and reported that  $I_{SAC}$  in atrial myocytes is permeable to  $Na^+$ ,  $K^+$ , and  $Ca^{2+}$  [33], and defined as

$$I_{SAC} = I_{SAC,Na} + I_{SAC,K} + I_{SAC,Ca}, \quad (4)$$

where  $I_{SAC,Na}$ ,  $I_{SAC,K}$ , and  $I_{SAC,Ca}$  represent the contributions of  $Na^+$ ,  $K^+$ , and  $Ca^{2+}$  to  $I_{SAC}$ , respectively. These currents are defined by the constant-field Goldman–Hodgkin–Katz current equation [56].

To introduce the effect of  $I_{SAC}$  on intracellular  $Na^+$ ,  $K^+$ , and  $Ca^{2+}$  concentrations ( $[Na^+]_i$ ,  $[K^+]_i$  and  $[Ca^{2+}]_i$ ), we replace equations of  $[Na^+]_i$ ,  $[K^+]_i$ , and  $[Ca^{2+}]_i$  in Maleckar et al.'s model [50] as

$$\frac{d[Na^+]_i}{dt} = -\frac{I_{Na} + I_{B,Na} + 3I_{NaK} + 3I_{NaCa} + I_{SAC,Na}}{Vol_i F} \quad (5)$$

$$\frac{d[K^+]_i}{dt} = -\frac{I_t + I_{Kur} + I_{K1} + I_{K,s} + I_{K,r} - 2I_{NaK} + I_{SAC,K}}{Vol_i F} \quad (6)$$

$$\frac{d[Ca^{2+}]_i}{dt} = -\frac{-I_{di} + I_{B,Ca} + I_{CaP} - 2I_{NaCa} + I_{up} - I_{rel} + I_{SAC,Ca}}{2.0Vol_i F} - \frac{dO}{dt}, \quad (7)$$

where  $F$  is Faraday's constant,  $Vol_i$  cytosolic volume,  $I_{di}$   $Ca^{2+}$  diffusion current from the diffusion-restricted subsarcolemmal space to the cytosol,  $I_{up}$  sarcoplasmic reticulum  $Ca^{2+}$  uptake current,  $I_{rel}$  sarcoplasmic reticulum  $Ca^{2+}$  release current, and  $O$  buffer occupancy.

### The model of the $Ca^{2+}$ -force relation

The model 4 of isometric force generation in cardiac myofilaments proposed by Rice et al. was adopted to model the  $Ca^{2+}$ -force relation [51, 52]. The concentration of  $Ca^{2+}$  bound to high-affinity or low-affinity troponin sites is [HTRPNCa] and [LTRPNCa], respectively. The dynamics are governed as

$$\frac{d[HTRPNCa]}{dt} = k_{\text{htprn}}^+ [Ca^{2+}]_i ([HTRPN]_{\text{tot}} - [HTRPNCa]) - k_{\text{htprn}}^- [HTRPNCa] \quad (8)$$

$$\frac{d[LTRPNCa]}{dt} = k_{\text{ltrpn}}^+ [Ca^{2+}]_i ([LTRPN]_{\text{tot}} - [LTRPNCa]) - k_{\text{ltrpn}}^- [LTRPNCa], \quad (9)$$

where  $[HTRPN]_{\text{tot}}$  represents the total troponin high-affinity site concentration, and  $k_{\text{htprn}}^+$  and  $k_{\text{htprn}}^-$  are the  $Ca^{2+}$  on- and off-rates for troponin high-affinity sites.  $[LTRPN]_{\text{tot}}$

represents the total troponin low-affinity site concentration, and  $k_{\text{trp}}^+$  and  $k_{\text{trp}}^-$  are the  $\text{Ca}^{2+}$  on- and off-rates for troponin low-affinity sites.

**The model of human atrial Mfb**

The electrophysiological model of human atrial Mfb proposed by MacCannell et al. [26] was used in the present study. It includes time- and voltage-dependent  $\text{K}^+$  current ( $I_{\text{Kv\_Mfb}}$ ), inward-rectifying  $\text{K}^+$  current ( $I_{\text{K1\_Mfb}}$ ),  $\text{Na}^+$ - $\text{K}^+$  pump current ( $I_{\text{NaK\_Mfb}}$ ), and  $\text{Na}^+$  background current ( $I_{\text{B,Na\_Mfb}}$ ).

In addition,  $I_{\text{Na\_Mfb}}$  and  $I_{\text{MGC\_Mfb}}$  are added in the Mfb model. According to our previous work [28], equations of  $I_{\text{Na\_Mfb}}$  and  $I_{\text{MGC\_Mfb}}$  are formulated as

$$I_{\text{Na\_Mfb}} = \bar{g}_{\text{Na,Mfb}} m_{\text{Mfb}} j_{\text{Mfb}}^{0.12} (V_{\text{Mfb}} - E_{\text{Na,Mfb}}) \tag{10}$$

$$E_{\text{Na,Mfb}} = \frac{RT}{F} \log \frac{[\text{Na}^+]_{\text{c,Mfb}}}{[\text{Na}^+]_{\text{i,Mfb}}} \tag{11}$$

$$I_{\text{MGC\_Mfb}} = \bar{g}_{\text{MGC,Mfb}} \cdot (V_{\text{Mfb}} - E_{\text{MGC,Mfb}}), \tag{12}$$

where  $\bar{g}_{\text{Na,Mfb}}$  is the maximum conductance of  $I_{\text{Na\_Mfb}}$  (0.756 nS),  $E_{\text{Na,Mfb}}$  the Nernst potential for  $\text{Na}^+$  ions,  $[\text{Na}^+]_{\text{c,Mfb}}$  the Mfb extracellular  $\text{Na}^+$  concentration (130.011 mM),  $[\text{Na}^+]_{\text{i,Mfb}}$  the Mfb intracellular  $\text{Na}^+$  concentration (the initial value is set as 8.5547 mM), and  $m_{\text{Mfb}}$  and  $j_{\text{Mfb}}$  the activation and inactivation parameters, respectively. To follow the experiment data [18],  $j$  has been modified as  $j^{0.12}$ .  $\bar{g}_{\text{MGC,Mfb}}$  is the maximum conductance of  $I_{\text{MGC\_Mfb}}$  (0.043 nS), and  $E_{\text{MGC,Mfb}}$  is the reversal potential of MGCs (selected a value close to 0 mV) [21].

**Mechanical behavior of a single segment**

The mechanical behavior of a single segment in our model is based on the classical three-element rheological scheme [53, 54].

As shown in Fig. 6, active force ( $F_{\text{CE}}$ ) is generated by the contractile element (CE), and passive forces ( $F_{\text{SE}}, F_{\text{PE}}$ ) are generated in a serial elastic element (SE) and a parallel elastic element (PE).  $F_{\text{segment}}$  is the total force generated by the segment. The element lengths are  $l_{\text{CE}}, l_{\text{SE}}$ , and  $l_{\text{PE}}$ . During mechanical equilibrium,  $F_{\text{CE}}, F_{\text{segment}}$ , and  $l_{\text{PE}}$  are defined as

$$F_{\text{CE}} = F_{\text{SE}} \tag{13}$$

$$F_{\text{segment}} = F_{\text{SE}} + F_{\text{PE}} \tag{14}$$

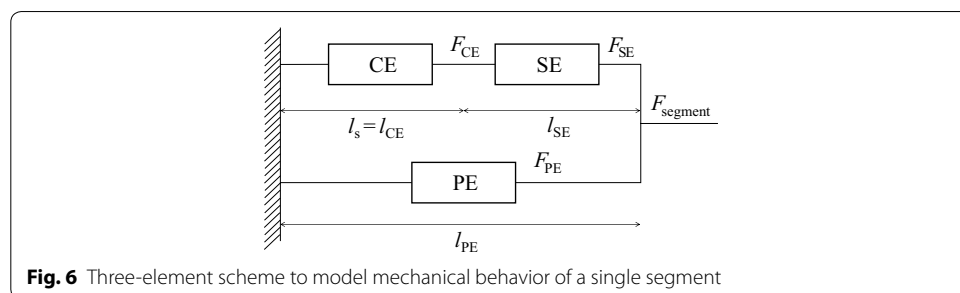


**Fig. 6** Three-element scheme to model mechanical behavior of a single segment

$$l_{PE} = l_{CE} + l_{SE}. \quad (15)$$

### Simulation protocol

We performed single-cell simulations with constant sarcomere length (isometric contraction) and constant applied force (isotonic contraction) to investigate the effects of  $I_{SAC}$ ,  $I_{Na\_Mfb}$ , and  $I_{MGC\_Mfb}$  on myocyte mechanical properties.

Five groups were simulated sequentially: one atrial myocyte without Mfb coupling (Group 1), one atrial myocyte coupled to two Mfbs without  $I_{SAC}$ ,  $I_{Na\_Mfb}$ , and  $I_{MGC\_Mfb}$  (Group 2), one atrial myocyte coupled to two Mfbs with  $I_{Na\_Mfb}$  (Group 3), one atrial myocyte coupled to two Mfbs with  $I_{SAC}$  and  $I_{Na\_Mfb}$  (Group 4), and one atrial myocyte coupled to two Mfbs with  $I_{SAC}$ ,  $I_{Na\_Mfb}$ , and  $I_{MGC\_Mfb}$  (Group 5).

First, simulations were carried out at a constant  $G_{gap}$  of 3 nS and a BCL of 1 s. Thereafter, the coupled system was paced with (1) BCLs from 0.1 to 2 s, (2)  $G_{gap}$  from 0.5 to 8 nS, and (3) number of coupled Mfbs from 1 to 8, to investigate the role of BCL,  $G_{gap}$ , and Mfbs in myocyte mechanical parameters. The maximum or minimum of  $F_{SE}$ ,  $F_{PE}$ ,  $F_{segment}$ ,  $l_{CE}$ ,  $l_{SE}$ , and  $l_{PE}$  at different BCL,  $G_{gap}$ , and Mfbs number were examined.

To ensure the coupled system reached steady-state, stimulation was repeated for 20 cycles. Results from the last cycle in each simulation were used for subsequent analyses. All state variables of the coupled model were updated by means of the forward Euler method. The time step was set to be 10  $\mu$ s to ensure numerical accuracy and stability. More information on “[Methods](#)” is available in the Additional file 1.

### Supplementary information

**Supplementary information** accompanies this paper at <https://doi.org/10.1186/s12938-019-0723-5>.

**Additional file 1.** Additional tables.

#### Abbreviations

SAC: stretch-activated channel; Mfb: myofibroblast; MGC: mechano-gated channel; Mfb-M: myofibroblast–myocyte; VGSC: voltage-gated sodium channel; AP: action potential; EMC: electromechanical coupling; MEF: mechano-electrical feedback; TRPM7: transient receptor potential cationic channel subfamily M member 7; APD: duration of the action potential; BCL: basic cycle length; CE: contractile element; SE: serial elastic element; PE: parallel elastic element.

#### Acknowledgements

Not applicable.

#### Authors' contributions

HZ prepared the manuscript in collaboration with the clinician (cardiologist) JZ. All authors read and approved the final manuscript.

#### Funding

This project is supported by the National Natural Science Foundation of China (81501557).

#### Availability of data and materials

All data generated or analyzed during this study are included in this article.

#### Ethics approval and consent to participate

Not applicable.

#### Consent for publication

We consent for the publication of this work.

#### Competing interests

The authors declare that they have no competing of interests.

**Author details**

<sup>1</sup> College of Medical Information, Hainan Medical University, Haikou 571199, China. <sup>2</sup> Cardiac Arrhythmia Center, Fuwai Hospital, National Center for Cardiovascular Diseases, Beijing 100037, China.

Received: 31 May 2019 Accepted: 16 October 2019

Published online: 25 October 2019

**References**

1. Trayanova NA, Boyle PM. Advances in modeling ventricular arrhythmias: from mechanisms to the clinic. *Wiley Interdiscipl Rev Syst Biol Med*. 2014;6(2):209–24.
2. Yang JH, Saucerman JJ. Computational models reduce complexity and accelerate insight into cardiac signaling networks. *Circ Res*. 2011;108(1):85–97.
3. Zaniboni M. Short-term action potential memory and electrical restitution: a cellular computational study on the stability of cardiac repolarization under dynamic pacing. *PLoS ONE*. 2018;13(3):e0193416.
4. Sato D, Dixon RE, Santana LF, Navedo MF. A model for cooperative gating of L-type  $\text{Ca}^{2+}$  channels and its effects on cardiac alternans dynamics. *PLoS Comput Biol*. 2018;14(1):e1005906.
5. Regazzoni F, Dede L, Quarteroni A. Active contraction of cardiac cells: a reduced model for sarcomere dynamics with cooperative interactions. *Biomech Model Mechanobiol*. 2018;17(6):1663–86.
6. Dupuis LJ, Lumens J, Arts T, Delhaas T. Mechano-chemical interactions in cardiac sarcomere contraction: a computational modeling study. *PLoS Comput Biol*. 2016;12(10):e1005126.
7. Pfeiffer ER, Tangney JR, Omens JH, McCulloch AD. Biomechanics of cardiac electromechanical coupling and mechano-electric feedback. *J Biomech Eng*. 2014;136(2):021007.
8. Zeng T, Bett GC, Sachs F. Stretch-activated whole cell currents in adult rat cardiac myocytes. *Am J Physiol Heart Circ Physiol*. 2000;278(2):H548–57.
9. Amar A, Zlochiver S, Barnea O. Mechano-electric feedback effects in a three-dimensional (3D) model of the contracting cardiac ventricle. *PLoS ONE*. 2018;13(1):e0191238.
10. Collet A, Bragard J, Dauby PC. Temperature, geometry, and bifurcations in the numerical modeling of the cardiac mechano-electric feedback. *Chaos*. 2017;27(9):093924.
11. Kohl P, Day K, Noble D. Cellular mechanisms of cardiac mechano-electric feedback in a mathematical model. *Can J Cardiol*. 1998;14(1):111–9.
12. Zeigler AC, Richardson WJ, Holmes JW, Saucerman JJ. Computational modeling of cardiac fibroblasts and fibrosis. *J Mol Cell Cardiol*. 2016;93:73–83.
13. Mouton AJ, Ma Y, Rivera Gonzalez OJ, Daseke MJ 2nd, Flynn ER, Freeman TC, Garrett MR, DeLeon-Pennell KY, Lindsey ML. Fibroblast polarization over the myocardial infarction time continuum shifts roles from inflammation to angiogenesis. *Basic Res Cardiol*. 2019;114(2):6.
14. Tarbit E, Singh I, Peart JN, Rose-Meyer RB. Biomarkers for the identification of cardiac fibroblast and myofibroblast cells. *Heart Fail Rev*. 2019;24(1):1–15.
15. Shibukawa Y, Chilton EL, Maccannell KA, Clark RB, Giles WR.  $\text{K}^{+}$  currents activated by depolarization in cardiac fibroblasts. *Biophys J*. 2005;88(6):3924–35.
16. Chilton L, Ohya S, Freed D, George E, Drobnic V, Shibukawa Y, Maccannell KA, Imaizumi Y, Clark RB, Dixon IM, Giles WR.  $\text{K}^{+}$  currents regulate the resting membrane potential, proliferation, and contractile responses in ventricular fibroblasts and myofibroblasts. *Am J Physiol Heart Circ Physiol*. 2005;288(6):H2931–9.
17. Du J, Xie J, Zhang Z, Tsujikawa H, Fusco D, Silverman D, Liang B, Yue L. TRPM7-mediated  $\text{Ca}^{2+}$  signals confer fibrogenesis in human atrial fibrillation. *Circ Res*. 2010;106(5):992–1003.
18. Chatelier A, Mercier A, Tremblier B, Theriault O, Moubarak M, Benamer N, Corbi P, Bois P, Chahine M, Faivre JF. A distinct de novo expression of Nav1.5 sodium channels in human atrial fibroblasts differentiated into myofibroblasts. *J Physiol*. 2012;590(17):4307–19.
19. Koivumäki JT, Clark RB, Belke D, Kondo C, Fedak PWM, Maleckar MMC, Giles WR.  $\text{Na}^{+}$  current expression in human atrial myofibroblasts: identity and functional roles. *Front Physiol*. 2014;5:275.
20. Li GR, Sun HY, Chen JB, Zhou Y, Tse HF, Lau CP. Characterization of multiple ion channels in cultured human cardiac fibroblasts. *PLoS ONE*. 2009;4(10):e7307.
21. Kamkin A, Kirischuk S, Kiseleva I. Single mechano-gated channels activated by mechanical deformation of acutely isolated cardiac fibroblasts from rats. *Acta Physiol*. 2010;199(3):277–92.
22. El Chemaly A, Guinamard R, Demion M, Fares N, Jebara V, Faivre JF, Bois P. A voltage-activated proton current in human cardiac fibroblasts. *Biochem Biophys Res Commun*. 2006;340(2):512–6.
23. Yue L, Xie J, Nattel S. Molecular determinants of cardiac fibroblast electrical function and therapeutic implications for atrial fibrillation. *Cardiovasc Res*. 2011;89(4):744–53.
24. Rohr S. Myofibroblasts in diseased hearts: new players in cardiac arrhythmias? *Heart Rhythm*. 2009;6(6):848–56.
25. Ashihara T, Haraguchi R, Nakazawa K, Namba T, Ikeda T, Nakazawa Y, Ozawa T, Ito M, Horie M, Trayanova NA. The role of fibroblasts in complex fractionated electrograms during persistent/permanent atrial fibrillation: implications for electrogram-based catheter ablation. *Circ Res*. 2012;110(2):275–84.
26. MacCannell KA, Bazzazi H, Chilton L, Shibukawa Y, Clark RB, Giles WR. A mathematical model of electrotonic interactions between ventricular myocytes and fibroblasts. *Biophys J*. 2007;92(11):4121–32.
27. McDowell KS, Vadakkumpadan F, Blake R, Blauer J, Plank G, Macleod RS, Trayanova NA. Mechanistic inquiry into the role of tissue remodeling in fibrotic lesions in human atrial fibrillation. *Biophys J*. 2013;104(12):2764–73.
28. Zhan H, Zhang J, Lin J, Han G. Effects of  $\text{Na}^{+}$  current and mechanogated channels in myofibroblasts on myocyte excitability and repolarization. *Comput Math Methods Med*. 2016;2016:6189374.

29. Reinhardt JW, Gooch KJ. Agent-based modeling traction force mediated compaction of cell-populated collagen gels using physically realistic fibril mechanics. *J Biomech Eng*. 2014;136(2):021024.
30. Checa S, Rausch MK, Petersen A, Kuhl E, Duda GN. The emergence of extracellular matrix mechanics and cell traction forces as important regulators of cellular self-organization. *Biomech Model Mechanobiol*. 2015;14(1):1–13.
31. Rouillard AD, Holmes JW. Coupled agent-based and finite-element models for predicting scar structure following myocardial infarction. *Prog Biophys Mol Biol*. 2014;115(2–3):235–43.
32. Fomovsky GM, Holmes JW. Evolution of scar structure, mechanics, and ventricular function after myocardial infarction in the rat. *Am J Physiol Heart Circ Physiol*. 2010;298(1):H221–8.
33. Kuijpers NH, ten Eikelder HM, Bovendeerd PH, Verheule S, Arts T, Hilbers PA. Mechanoelectric feedback leads to conduction slowing and block in acutely dilated atria: a modeling study of cardiac electromechanics. *Am J Physiol Heart Circ Physiol*. 2007;292(6):H2832–53.
34. Zhan HQ, Xia L. Excitation-contraction coupling between human atrial myocytes with fibroblasts and stretch activated channel current: a simulation study. *Comput Math Methods Med*. 2013. <https://doi.org/10.1155/2013/238676>.
35. Franz MR, Burkhoff D, Yue DT, Sagawa K. Mechanically induced action potential changes and arrhythmia in isolated and in situ canine hearts. *Cardiovasc Res*. 1989;23(3):213–23.
36. Isenberg G, Kazanski V, Kondratev D, Gallitelli MF, Kiseleva I, Kamkin A. Differential effects of stretch and compression on membrane currents and  $[Na^+]_i$  in ventricular myocytes. *Prog Biophys Mol Biol*. 2003;82(1–3):43–56.
37. van Putten S, Shafeyan Y, Hinz B. Mechanical control of cardiac myofibroblasts. *J Mol Cell Cardiol*. 2016;93:133–42.
38. Hinz B, Phan SH, Thannickal VJ, Galli A, Bochaton-Piallat ML, Gabbiani G. The myofibroblast: one function, multiple origins. *Am J Pathol*. 2007;170(6):1807–16.
39. Wang H, Abhilash AS, Chen CS, Wells RG, Shenoy VB. Long-range force transmission in fibrous matrices enabled by tension-driven alignment of fibers. *Biophys J*. 2014;107(11):2592–603.
40. Harris AK, Stopak D, Wild P. Fibroblast traction as a mechanism for collagen morphogenesis. *Nature*. 1981;290(5803):249–51.
41. Rouillard AD, Holmes JW. Mechanical regulation of fibroblast migration and collagen remodelling in healing myocardial infarcts. *J Physiol*. 2012;590(18):4585–602.
42. Fomovsky GM, Rouillard AD, Holmes JW. Regional mechanics determine collagen fiber structure in healing myocardial infarcts. *J Mol Cell Cardiol*. 2012;52(5):1083–90.
43. Catterall WA, Goldin AL, Waxman SG. International Union of Pharmacology. XLVII. Nomenclature and structure–function relationships of voltage-gated sodium channels. *Pharmacol Rev*. 2005;57(4):397–409.
44. Kamkin A, Kiseleva I, Isenberg G, Wagner KD, Gunther J, Theres H, Scholz H. Cardiac fibroblasts and the mechano-electric feedback mechanism in healthy and diseased hearts. *Prog Biophys Mol Biol*. 2003;82(1–3):111–20.
45. Kamkin A, Kiseleva I, Lozinsky I, Scholz H. Electrical interaction of mechanosensitive fibroblasts and myocytes in the heart. *Basic Res Cardiol*. 2005;100(4):337–45.
46. Herum KM, Lunde IG, McCulloch AD, Christensen G. The soft- and hard-heartedness of cardiac fibroblasts: mechanotransduction signaling pathways in fibrosis of the heart. *J Clin Med*. 2017;6(5):53.
47. Zlochiver S, Munoz V, Vikstrom KL, Taffet SM, Berenfeld O, Jalife J. Electrotonic myofibroblast-to-myocyte coupling increases propensity to reentrant arrhythmias in two-dimensional cardiac monolayers. *Biophys J*. 2008;95(9):4469–80.
48. Reed A, Kohl P, Peyronnet R. Molecular candidates for cardiac stretch-activated ion channels. *Glob Cardiol Sci Pract*. 2014;2014(2):9–25.
49. Rog-Zielinska EA, Norris RA, Kohl P, Markwald R. The living scar-cardiac fibroblasts and the injured heart. *Trends Mol Med*. 2016;22(2):99–114.
50. Maleckar MM, Greenstein JL, Giles WR, Trayanova NA.  $K^+$  current changes account for the rate dependence of the action potential in the human atrial myocyte. *Am J Physiol Heart Circ Physiol*. 2009;297(4):H1398–410.
51. Rice JJ, Jafri MS, Winslow RL. Modeling short-term interval-force relations in cardiac muscle. *Am J Physiol Heart Circ Physiol*. 2000;278(3):H913–31.
52. Rice JJ, Winslow RL, Hunter WC. Comparison of putative cooperative mechanisms in cardiac muscle: length dependence and dynamic responses. *Am J Physiol*. 1999;276(5 Pt 2):H1734–54.
53. Hill AV. The heat of shortening and the dynamic constants of muscle. *Proc R Soc Lond Ser B*. 1938;126:136.
54. Solovyova O, Katsnelson L, Guriev S, Nikitina L, Protsenko Y, Routkevitch S, Markhasin V. Mechanical inhomogeneity of myocardium studied in parallel and serial cardiac muscle duplexes: experiments and models. *Chaos Soliton Fract*. 2002;13(8):1685–711.
55. Kim D. Novel cation-selective mechanosensitive ion channel in the atrial cell membrane. *Circ Res*. 1993;72(1):225–31.
56. Keener JP, Sneyd J. *Mathematical physiology*. New York: Springer; 1998.

## Publisher's Note

Springer Nature remains neutral with regard to jurisdictional claims in published maps and institutional affiliations.